Domain Motions and the Open-to-Closed Conformational Transition of an Enzyme: A Normal Mode Analysis of *S*-Adenosyl-L-homocysteine Hydrolase†

Mengmeng Wang,‡ Ronald T. Borchardt,§ Richard L. Schowen,‡,§ and Krzysztof Kuczera*,‡,||

Department of Chemistry, Department of Molecular Biosciences, and Department of Pharmaceutical Chemistry, The University of Kansas, Lawrence, Kansas 66045

Received November 24, 2004; Revised Manuscript Received March 11, 2005

ABSTRACT: The structure and fluctuations of the enzyme *S*-adenosyl-L-homocysteine hydrolase (SAHH) are analyzed in an effort to explain its biological function. Besides the previously identified open structure, characteristic of the substrate-free enzyme, we find two distinct structures in enzyme−inhibitor complexes, the closed and closed−twisted conformers. Both closed conformers differ from the open form by a hinge bending motion of two large domains within each subunit, which isolate the inhibitor bound in the active site from the bulk solvent. The closed−twisted form further differs from the closed form by a rigid body twist of the two-subunit dimers. The local structural fluctuations of SAHH are analyzed by performing block normal mode analysis of the tetrameric enzyme in its three forms. For the open form, we find that the four lowest-frequency normal modes, corresponding to the collective motions of the protein with the largest amplitudes, are essentially combinations of the hinge bending deformations of the individual subunits. Thus, the mechanical properties of the open structure of SAHH lead to the presence of structural fluctuations in the direction of the open-to-closed conformational transition. A candidate for such a motion has been observed in previous fluorescence depolarization studies of the enzyme. Both structural and normal mode analyses indicate that residues 180−190 and 350−356 form hinge regions, connecting large domains which tend to move as rigid bodies in response to interactions with substrate, intermediates, and the product of the enzymatic reactions. We propose that these hinge regions play a crucial role in the enzymatic mechanism of SAHH. In contrast to the open form, normal mode calculations for the closed conformations show strong coupling of the hinge bending motions of the individual subunits to each other and to other low-frequency vibrations. Thus, information about structural changes related to reaction progress in one active site may be mechanically transmitted to other subunits of the protein, explaining the cooperativity found in the enzyme kinetics.

S-Adenosyl-L-homocysteine hydrolases (SAHHs,[1] EC 3.3.1.1) in mammalian cells and parasites play key roles in controlling the intracellular levels of adenosyl-L-homocysteine (AdoHcy) by catalyzing its metabolism to homocysteine (Hcy) and adenosine (Ado). By controlling intracellular levels of AdoHcy, this enzyme plays a pivotal role in regulating *S*-adenosyl-L-methionine (AdoMet)-dependent methyltransferases, which are crucial for the viability of mammalian and parasite cells. In humans, high Hcy levels appear to be risk factors for cardiovascular diseases (*1*, *2*). In eukaryotic cells, SAHH is the enzyme that catalyzes the only known pathway for the catabolism of AdoHcy. Therefore, SAHH is a target for antiviral (*3*) and antiparasitic (*4*) drugs.

SAHH is a homotetramer (Figure 1A) with a cofactor NAD bound in each of its four identical active sites (*5*). Each subunit consists of three domains: the N-terminal substrate-binding domain, the cofactor-binding domain, and a small C-terminal "tail". The tail of subunit A protrudes into the adjacent subunit B and forms part of the cofactor-binding site in that subunit. Reciprocally, the tail from subunit B protrudes into subunit A. An analogous linkage through exchange of tails exists between subunits C and D. The tetrameric SAHH is therefore a "dimer of dimers", formed by the tightly coupled A−B and C−D dimers. The four cofactor-binding domains together form a central core of the tetramer structure, with the substrate-binding domains exposed on the surface.

Initial structural analysis of SAHH identified the presence of two conformers, denoted as open and closed (*6*). The substrate-free, NAD^+ form of SAHH exists in the open conformation, with an open cleft between the substrate-binding domain (SBD) and cofactor-binding domain (CBD) within each subunit (Figure 1C). Once the substrate analogue 2′,3′-dihydroxycyclopen-4′-enyladenine (DHCeA) binds and the cofactor is reduced to NADH, the enzyme exists in the

† This work was supported by National Institutes of Health Grant GM-29332.

* To whom correspondence should be addressed: Departments of Chemistry and Molecular Biosciences, University of Kansas, 1251 Wescoe Hall Dr., Lawrence, KS 66045. Telephone: (785) 864-5060. Fax: (785) 864-5396. E-mail: kkuczera@ku.edu.

‡ Department of Chemistry.

§ Department of Molecular Biosciences.

|| Department of Pharmaceutical Chemistry.

[1] Abbreviations: SAHH, *S*-adenosyl-L-homocysteine hydrolase; AdoHcy, adenosyl-L-homocysteine; Hcy, homocysteine; Ado, adenine; SBD, substrate-binding domain; CBD, cofactor-binding domain; BNM, block normal mode; ABNR, adopted basis Newton−Raphson; rmsd, root-mean-square deviation; DHCeA, 2′,3′-dihydroxycyclopen-4′-enyladenine.

10.1021/bi047524m CCC: $30.25
Published on Web 04/23/2005

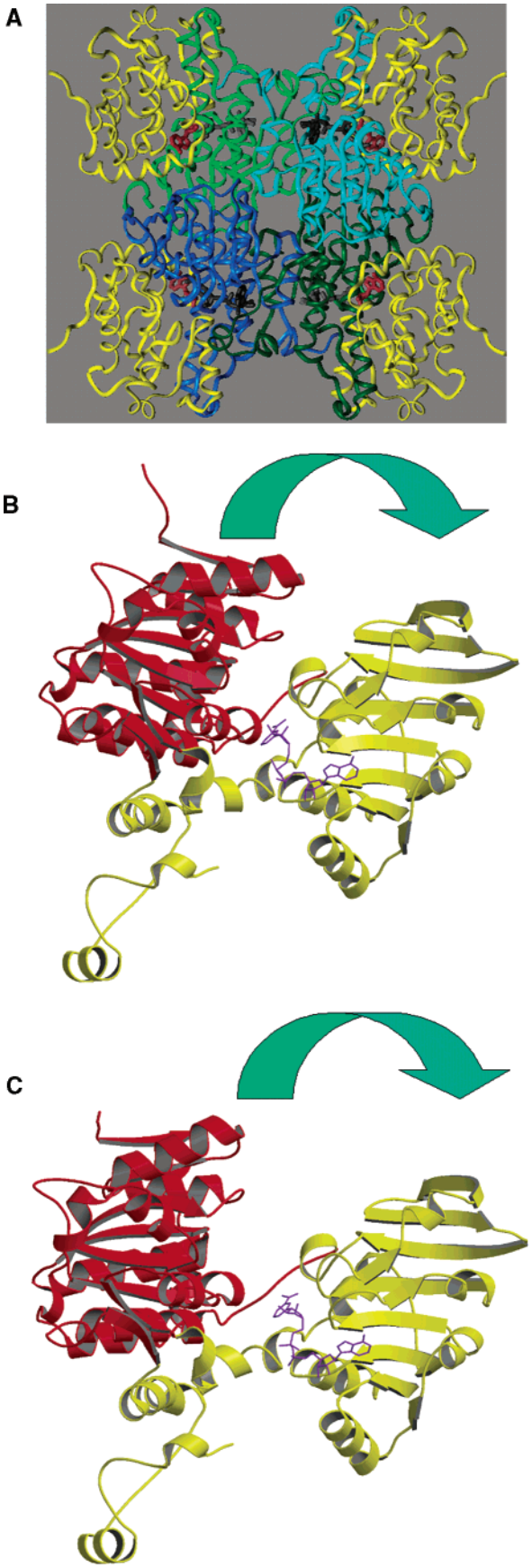

FIGURE 1: Structure of the SAHH (A) tetramer of closed form 1A7A (*5*). (B) Subunit A of closed form 1A7A, with the substrate-binding domain colored red, the cofactor binding domain yellow, and the cofactor purple (*15*). (C) Subunit A of open form 1KY4 (*6*), with colors as in panel B. The direction of hinge bending motion is shown with an arrow.

closed form, in which the two large domains have come together, with the oxidized inhibitor deeply engulfed at their interface (Figure 1B). Comparison of the two structures shows that the SBD and CBD remain essentially internally unchanged, and that the conformational change can be described by two kinds of rigid body motions (*6*). The first is a hinge bend involving an 18° rotation of the SBD relative to the CBD within each subunit. The second motion involves a reorientation of the A−B dimer relative to the C−D dimer by 14° (*6*). Subsequent systematic analysis of crystal structures of SAHH−inhibitor complexes indicated the existence of two distinguishable closed forms, which differ in the distance between the inhibitor and cofactor (*7*). Further insight into the structural transitions of SAHH was obtained by fluorescence depolarization studies, which discovered a motion that occurs on a 25 ns time scale in the substrate-free enzyme and is abolished by addition of an inhibitor (*8*). On the basis of the probe attachment site in the substrate-binding domain and the known crystal structures, this motion was assigned as the hinge-bending domain reorientation. Thus, our current understanding of the conformational dynamics of SAHH is that in the substrate-free state it exists as the open form, while exhibiting oscillation along the direction of the open-to-closed conformational transition with a frequency of $\sim 4 \times 10^7$ s^{-1}. The crystallographic and fluorescence studies show that binding of inhibitor, which arrests the protein at an intermediate stage of the enzymatic reaction, induces a transition to the closed form. We believe that in the course of the normal reaction, substrate binding also induces the open-to-closed transition in SAHH, and the enzymatic reaction occurs in the active site sequestered from solvent, followed by the transition to the open form and product release (*7*).

On the basis of this analysis, it is clear that the open-to-closed structural transition is a key feature of enzymatic activity of SAHH, enabling diffusion of the substrate into and the product out of the active site, as well as creating sequestered conditions for the enzymatic reaction steps. Such transitions are of general importance for the function of many proteins (*9*). Previous crystallographic and fluorescence studies have provided important information about SAHH structure and dynamics. In this work, we present an investigation of the properties of the different conformers of this interesting protein.

We first perform an analysis of the existing crystal structures to describe three distinct SAHH conformations: open, closed, and closed−twisted. Subsequently, to improve our understanding of the properties of the SAHH conformers and to gain insight into the nature of the transitions between them, we model the large-amplitude low-frequency motions in this protein. Two standard approaches to modeling macromolecular motions, molecular dynamics simulations and normal mode analysis (*10*−*12*), cannot easily be applied to SAHH due to its large size, 1728 residues. To make calculations for our large protein tractable, we have chosen to use the block normal modes method (BNM) (*13*, *14*), which uses the full atomic force field to calculate the low-frequency normal modes in a reduced representation of the system. Using the BNM approach, we generate the atomic motions corresponding to low-frequency large-amplitude vibrations of SAHH to analyze the structural fluctuations of three conformers and coupling between movements of the

individual domains and subunits of the protein. Finally, we draw conclusions about the relation between structural fluctuations within the conformers, structural transitions between them, and SAHH catalytic function.

METHODS

Preparation of Models. The starting atomic coordinates for *S*-adenosyl-L-homocysteine hydrolase used in this study were as follows: human SAHH with NADH as a cofactor and DHCeA as an inhibitor for the closed−twisted conformation [PDB entry 1A7A (*5*)], rat SAHH with NAD^+ as a cofactor and with bound inhibitor D-Eritadenine for the closed conformation [PDB entry 1K0U (*15*)], and rat SAHH with NAD^+ as a cofactor for the open conformation [PDB entry 1KY4 (*6*)]. SAHH is a tetramer with 432 residues in each subunit, but the first couple of residues were not located in the crystal structures. We built the missing residues in an extended conformation using CHARMM (*16*). Water molecules were not included in the models. The inhibitor in 1K0U was removed, and polar hydrogens were added to the molecules with the HBUILD (*17*) function of CHARMM. Energy minimizations were performed in vacuo using the adopted basis Newton−Raphson (ABNR) algorithm (*16*). To avoid large shifts away from the experimental structures and remove any initial strain, initial energy minimization involved harmonic constraints on all atoms. At this stage, 17 cycles of 100 steps of ABNR minimization were applied, with harmonic force constants progressively decreasing in magnitude from 500 to 5 kcal mol^{-1} $Å^{-2}$ for backbone and from 100 to 1 kcal mol^{-1} $Å^{-2}$ for side chains. This was followed by roughly 10 000 cycles of unrestrained minimization, until the energy gradient was less than 10^{-4} kcal mol^{-1} $Å^{-1}$. After minimizations, the backbone atom root-mean-square deviation (rmsd) from the corresponding starting structures was 1.1 Å for the closed form and 0.9 Å for the open form. The CHARMM version 22 all-atom protein force field was employed (*18*) with the NAD^+ force field taken from ref *19*.

Block Normal Mode Analysis. In block normal mode (BNM) analysis, a large system of N atoms is coarse-grained by dividing the structure into n_b blocks (*13*). Typically, the blocks may be made up of one or more consecutive residues. The low-frequency modes of the protein are calculated as linear combinations of the rigid-body translations and rotations (T/R) of the blocks, i.e., with fixed internal structure inside the blocks. A subspace Hessian matrix ($\mathbf{H}^{sub}$) is constructed in the basis of the block rotations and translations:

$$\mathbf{H}^{sub} = \mathbf{P}^T \cdot \mathbf{H} \cdot \mathbf{P}$$

where $\mathbf{H}$ is the standard Hessian matrix, i.e., the $3N \times 3N$ matrix of the second derivatives of the potential energy with respect to the mass-weighted Cartesian coordinates, $\mathbf{P}$ is a $3N \times 6n_b$ projection matrix from the full space of $3N$ atomic coordinates to the $6n_b$ vectors associated with the local block rotations and translations (*20*), and the superscript T denotes a matrix transpose. The dimension of the reduced Hessian matrix, $\mathbf{H}^{sub}$, is $6n_b \times 6n_b$. Diagonalization of $\mathbf{H}^{sub}$ gives the vibrational frequencies ($^1/_2\pi\Lambda^{1/2}$) and eigenvectors ($\mathbf{U}^{sub}$) in the block T/R basis

$$[\mathbf{U}^{sub}]^T \cdot \mathbf{H}^{sub} \cdot [\mathbf{U}^{sub}] = \Lambda$$

The eigenvectors in the T/R subspace can be converted to the atomic space ($\mathbf{U}$) using the transpose of the projection matrix, $\mathbf{P}$

$$\mathbf{U} = \mathbf{P}^T \cdot \mathbf{U}^{sub}$$

The low-frequency normal mode vectors obtained in this way are very close to those generated by diagonalization of the full $3N \times 3N$ Hessian $\mathbf{H}$. The frequencies calculated in the BNM approach tend to be underestimated and are corrected by an empirical scaling factor to approximately agree with full Hessian results (*14*).

Atomic Fluctuations and Covariance Matrices. In the harmonic approximation, the atomic fluctuations may be described by the covariance matrix $\mathbf{C}$:

$$C_{ij} = \langle \Delta\vec{R}_i \cdot \Delta\vec{R}_j \rangle = k_B T \sum_{k=1}^{n_\nu} \frac{a_{ij}^k}{\omega_k^2}$$

where ΔR_i is the Cartesian displacement of atom i from its equilibrium position, k_B is the Boltzmann constant, T is the temperature, n_ν is the number of modes considered, $\upsilon_k = \omega_k/2\pi$, the frequency of normal mode k, and the normal mode overlap is

$$a_{ij}^k = L_{ix,k}L_{jx,k} + L_{iy,k}L_{jy,k} + L_{iz,k}L_{jz,k}$$

with $L_{ix,k}$ being the eigenvector element describing the amplitude of motion of atom i along the x axis in the kth vibrational eigenvector, etc. The diagonal elements of $\mathbf{C}$ describe the mean-square atomic fluctuations, while the off-diagonal elements describe the correlations between the fluctuations of atom pairs. For the purposes of visualizing the correlations in atomic fluctuations, we present plots of the normalized covariance matrices

$$C'^k_{ij} = \frac{C^k_{ij}}{\sqrt{C^k_{ii} C^k_{jj}}}$$

where C^k is the contribution from mode k to $\mathbf{C}$ as defined above.

Normal Mode Projections. To obtain projections of individual modes of structure X on the direction of the conformational transition between structures X and Y, structure Y was reoriented by backbone overlay on structure X. Next, the dot products were calculated between the $3N$-dimensional Cartesian normal mode vectors of X and the displacement vector obtained from the atomic coordinate differences between overlaid structures X and Y.

Normal Mode Animations. To analyze the nature of the concerted protein motions corresponding to the lowest-frequency vibrations, we used the BNM eigenvectors to generate normal mode trajectories. From these trajectories, computer animations were generated for graphical analysis of the low-frequency motions. The movies may be viewed at our Web site (*21*). For the open form of the enzyme, we performed an additional analysis of the four lowest-frequency normal mode trajectories using CHARMM, as follows. For a given subunit (say subunit A), for each trajectory snapshot,

Table 1: Comparison of SAHH Structures

		1K0U−1KY4	1A7A−1KY4	1A7A−1K0U	1IL4−1KY4	1KY5−1KY4
subunit A	BB[a]	2.79	2.90	0.71	2.77	2.93
	CAD[b]	0.41	0.42	0.28	0.44	0.41
	NBD[c]	0.32	0.29	0.28	0.24	0.32
	open−closed angle[d]	16.8	18.5	1.7	17.8	18.2
tetramer	NBD superimposed[e]	1.41	1.59	1.55	0.40	0.45
	NBD (A−B)[f]	0.38	0.36	0.30	0.36	0.45
	NBD (C−D)[g]	0.35	0.35	0.30	0.36	0.41
	twisting angle[h]	0.8	13.8	13.4	0.67	0.75

[a] Backbone rms deviation of overlaid A subunits, in angstroms. [b] Backbone rms deviation of overlaid substrate-binding domains (SBD, residues 5−180 and 357−374), in angstroms. [c] Backbone rms deviation of overlaid cofactor-binding domains (CBD, residues 191−356), in angstroms. [d] Reorientation angle upon a change between overlaying SBDs and CBDs, in degrees (hinge bend). [e] Backbone rms deviation of overlaid CBDs of the tetramer. [f]Backbone rms deviation of overlaid CBDs of the A−B dimer, in angstroms. [g] Backbone rms deviation of overlaid CBDs of the C−D dimer, in angstroms. [h] Reorientation angle upon a change between overlaying CBDs of A−B and C−D dimers, in degrees (dimer twist).

first the cofactor binding domain and then the substrate-binding domain were overlaid (in the backbone rmsd sense) on the energy-minimized structure. The coordinate transformation reported by CHARMM for this last overlay operation was recorded. In the general case, the overlay is described by a translation and rotation of the moving atoms and by the rmsd between the two coordinate sets. In our case, we found this operation corresponded to a pure rigid-body displacement of the substrate-binding domain around an axis passing through its center of mass. This method led to the determination of a unique rotation axis for each of the four subunits (A−D), the same axis for snapshots with different displacement amplitudes from equilibrium and for the four normal modes. Thus, the motions within the four lowest-frequency modes of the open form of SAHH correspond to different combinations of the same rigid-body rotations of the four substrate-binding domains. Further, we compared the rotation axes obtained from the mode animations to those corresponding to the overlay of the SB on the CB domains of the subunits in the starting energy-minimized structures of SAHH. The two sets of axes were very similar, with the magnitude of the dot products of their unit vectors being >0.95 for all subunits. Thus, the rotation axes describing the domain motions within the normal modes form an angle of only 18° with the axes obtained for the closed-to-open structural transition (see the introductory section).

Hinge Bending Force Constant Calculations. Because of the high degree of similarity between the domain hinge bending motions in the open form normal modes and the closed-to-open structural transition, it is possible to determine the approximate force constants for the hinge bending motions. Our procedure was as follows. From the calculations outlined in the previous section, we obtained the reorientation angles of the SB domains along the normal mode trajectories, obtaining sinusoidal traces, as expected. From the maximum values of the angles, we determined the coefficients of the linear combinations:

$$q_k = \sum_i A_{ki} \Delta u_i \text{ or } q = \mathbf{A}\Delta u$$

where Δu_i (i = A, B, C, or D) values are the displacements from equilibrium of the SBD reorientation angles in the four subunits and q_k ($k = 7, 8, 9$, or 10) values are the four lowest-frequency vibrational modes. Next, for each mode, the potential energy was calculated along the trajectory and the region close to $q = 0$ was fitted to a $V_k = {}^1/_2 f_k q_k^2$ parabola to determine the normal mode force constants f_k. The force constant matrix in the hinge bending coordinates was then determined as

$$F_{u,ij} = \sum_{ij} f_k A_{ik} A_{jk} \text{ or } \mathbf{F}_u = \mathbf{A}^T \cdot \mathbf{F}_q \cdot \mathbf{A}$$

where $F_{q,kl} = f_k \delta_{kl}$ is the diagonal force constant matrix in the normal mode coordinates and δ_{kl} is the Kronecker symbol. The covariance matrix describing the fluctuations in the subspace of the hinge bending deformations ($C_{u,ij} = \langle \Delta u_i \Delta u_j \rangle$) is calculated in the standard way

$$\mathbf{C}_u = k_B T \cdot \mathbf{F}_u^{-1}$$

RESULTS AND DISCUSSION

Three Structural States of SAHH

There are currently five different crystal structures of SAHH available in the Protein Data Bank, one for the substrate-free form, 1KY4 (*6*), and four of complexes with inhibitors, 1A7A (*5*), 1K0U (*15*), 1LI4 (*7*), and 1KY5 (*22*). The substrate-free enzyme structure 1KY4, denoted as the open conformation, has the cofactor in the NAD^+ form. This structure was determined for the rat enzyme, the sequence of which is 97% identical with the human protein (*6*). The 1A7A structure was determined for the human enzyme treated with the substrate analogue 2′,3′-dihydroxycyclopen-4′-enyladenine (DHCeA), which was bound and oxidized, arresting the enzyme in the NADH state (*5*). The 1K0U structure is a complex of the rat enzyme with the inhibitor D-Eritadenine, an acyclic sugar analogue of adenosine, with the cofactor in the NAD^+ state. 1LI4 is a complex of the human enzyme with the cofactor in the NAD^+ form and with inhibitor NepA in its 3′-keto form (*7*), another analogue of the intermediate 4′,5′-didehydro-5′-deoxy-3′-ketoadenosine. Structure 1KY5 is a D244E mutant of the rat liver enzyme with weakly bound NADH, complexed with 3′-keto-adenosine, with 50% occupancy of the inhibitor and cofactor (*22*).

A comparison of the crystal structures by overlay of domains, subunits, and dimers is presented in Table 1. It is clear that the large domains of SAHH take on essentially identical three-dimensional structures in all five crystal structures, with backbone root-mean square deviations (rmsd's) of 0.3 Å between all enzyme−inhibitor complexes and the substrate-free form. These differences are comparable to the errors in coordinate determination (*7*).

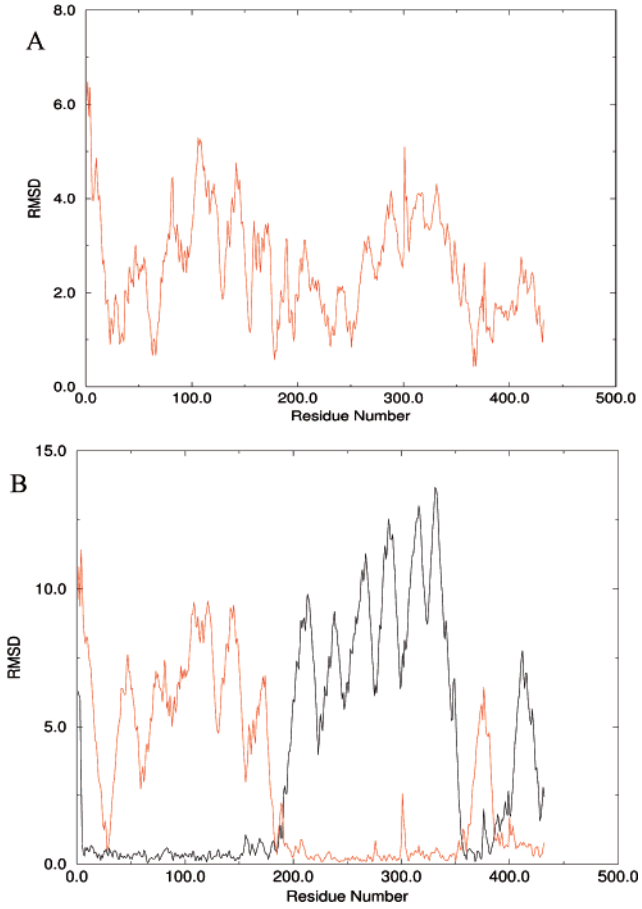

FIGURE 2: Backbone rms deviations between the open (1KY4) and closed (1K0U) forms of SAHH, in angstroms. (A) Overlay of whole subunit A (residues 1−432). (B) Overlay of the cofactor-binding domains (residues 182−351 and 386−432) (red) and substrate-binding domains (residues 5−181 and 355−385) (blue).

At the subunit level, there are significant differences (rmsd = 2.8−2.9 Å) between the conformations of the complexes and the substrate-free form 1KY4. From Table 1, we can see that these differences are due essentially to rigid body motions of the two large domains. Thus, for the 1K0U−1KY4 pair, starting in an orientation with the SBDs of subunit A overlaid, the overlay of the CBDs of subunit A is achieved through a translation by 4 Å and a rotation by 16.8°. The analogous operation for the 1A7A−1KY4 pair involves a translation by the same 4 Å and rotation by 18.5°. The orientation change between structures with overlaid CBDs and SBDs leaves unchanged two regions of each subunit, residues 182−186 and 351−356 (Figure 2). Thus, we can think of the subunit level structural changes between the substrate-free enzyme and inhibitor complexes as hinge bending motions of the domains, with residues 182−186 and 351−356 as the hinges connecting the rigid domains. The subunit structure of the substrate-free form is characterized by an open cleft between the substrate-binding and cofactor-binding domains. This cleft is closed, sequestering the active site from bulk solvent in the inhibitor complexes. The open and closed subunit structures are shown in Figure 1.

The subunit structures in inhibitor complexes 1A7A and 1K0U are quite similar, with a backbone rmsd of only 0.7 Å. However, the rmsd of the large domains may be lowered by a small rigid body movement, corresponding to a translation of 0.4 Å and a rotation of 1.7°. Interestingly, the hinge bending motions accompanying the transitions from 1KY4 to 1K0U (16.8°) and then from 1K0U to 1A7A (1.7°) add up to the hinge bend between 1KY4 and 1A7A (18.5°). We can thus consider the subunits of 1A7A to be 1.7° more tightly closed than those of 1K0U.

The similarity of the structures of the nucleotide-binding domains is maintained at the levels of the subunit dimers, with rmsd's between dimer NBDs of 0.3−0.4 Å for the A−B and C−D dimers (Table 1). At the tetramer level, DHCeA complex 1A7A stands out as having dimer orientations different than those of the substrate-free form 1KY4 and the eritadine complex 1K0U. If one starts with an orientation in which the NBDs of the A−B dimer are overlaid, the NBDs of CD may be overlaid through a translation by 1.9 Å and a rotation of 13.4° for the 1A7A−1K0U pair, and a translation by 1.9 Å and a rotation of 13.8° for the 1A7A−1KY4. In turn, the dimers of 1KY4 and 1K0U differ only by a translation of 0.2 Å and a rotation of 0.8° (Table 1).

On the basis of the analysis described above, we can identify three major conformations of the enzyme. The substrate-free form of the enzyme has been crystallized in the open conformation, with an open binding cleft between the substrate-binding and cofactor-binding domains, as seen in 1KY4 (Figure 1C). The eritadine complex 1K0U, which corresponds to either the enzyme−substrate or enzyme−product complex in the enzymatic cycle, with the oxidized form of the cofactor, exhibits a closed conformation (Figure 1B). Here the domain cleft is closed, and dimer orientations remain very similar to those of the open form. Finally, DHCeA complex 1A7A, corresponding to the central intermediate of the enzymatic cycle and the reduced NADH form of the cofactor, takes on the closed−twisted conformation, with the domain cleft a little more tightly closed than that of 1K0U, and with the dimers rotated by ~14° compared to both open and closed structures.

In terms of dimer orientations, the remaining enzyme−inhibitor complexes, 1KY5 and 1LI4, occupy closed structures similar to 1K0U. The dimer twists relative to 1KY4 are 0.8° for 1KY5 and 0.7° for 1LI4, similar to the twist of 0.8° found for 1K0U. Thus, the dimer orientations of 1KY5, 1LI4, and 1K0U are very similar to each other and to substrate-free form 1KY4. In terms of the extent of the interdomain hinge closure, the enzyme−inhibitor complexes appear to fall into two classes. The 1K0U complex, which corresponds to either the initial enzyme−substrate or the final enzyme−product complex, exhibits the smallest extent of hinge closing, with a bend angle of 16.8°. The other three complexes exhibit hinge closures in the range of 17.8−18.5° (Table 1). The 1A7A and 1LI4 complexes correspond to the central intermediate 4′,5′-didehydro-5′-deoxy-3′-ketoadenosine of the enzymatic cycle, while 1KY5 corresponds to a state at the end of the elimination step. The more tightly closed hinges in these three structures appear to be the subunit level effects of the conformational changes previously observed in an analysis of the active sites (*7*).

Thus, our current understanding of the conformational dynamics of SAHH is that in the substrate-free state the protein exists as the open form, able to bind substrate in the open interdomain clefts of its subunits. Fluorescence depolarization studies show that in this state the substrate-binding domains of SAHH, which are oriented toward the exterior of the protein, exhibit motions with a time scale of ~25 ns.

Table 2: Four Lowest Vibrational Frequencies of the Conformers of SAHH Calculated from BNM (cm^{-1})

	mode 7	mode 8	mode 9	mode 10
1K0U[a]	2.58	2.94	3.00	3.11
1KY4[b]	1.35	1.46	1.67	1.68
1A7A[c]	1.81	2.00	2.31	2.60

[a] 1K0U is the closed form. [b] 1KY4 is the open form. [c] 1A7A is the closed−twisted form.

It is tempting to speculate that the domain motions of the open form occur along the direction of the open-to-closed structural transition, but there is no experimental evidence to support this hypothesis. The crystallographic structures of the SAHH−inhibitor complexes may be thought to represent various intermediates in the enzymatic reaction. Structural analysis suggests that substrate binding proceeds in two stages. Initial substrate binding triggers a transition to the closed conformation, with a closed interdomain cleft and the substrate sequestered from the bulk solvent. Subsequently, perhaps in concert with or immediately following the oxidation step, the enzyme appears to undergo a second conformational change. This transition involves a small additional closure of the domain hinge by 1−2°, as found in 1A7A and 1LI4 representing the central intermediate and 1KY5 representing the stage after the elimination step. As previously recognized on the basis of the structure analysis of the active sites, the additional hinge closing induces an elongation of the substrate−cofactor distance of ~0.4 Å (*6*). This promotes the occurrence of the oxidative step of the enzymatic reaction after initial substrate binding to SAHH and suppresses the abortive reduction of the central intermediate, 4′,5′-didehydro-5′-deoxy-3′-ketoadenosine (*6*). It is tempting to suggest that the small additional closure occurs at the same time as the dimer twist. However, as the dimer twist is only found in the 1A7A structure and not in 1LI4, it is not possible to determine if this kind of motion is important for the catalytic mechanism of SAHH, or whether it is a structural transition induced by the crystal environment. Accordingly, the relevance of the closed−twisted structure for SAHH activity remains unknown at present.

In the following sections, we present the results of normal mode analysis of the three conformers of SAHH, aimed at exploring the nature of their structural fluctuations. Interestingly, the open and closed structures exhibit markedly different low-frequency, large-amplitude collective motions. These results suggest the identity of the domain motion observed in the fluorescence experiments, uncover correlations between structural fluctuations of SAHH subunits and domains, and provide further insights into the catalytic mechanism of this interesting enzyme.

Block Normal Mode Analysis

The first 100 low-frequency modes of the open, closed, and closed−twisted forms of tetrameric SAHH were calculated using the block normal mode (BNM) method. The results are presented below.

BNM Frequencies. The lowest vibrational frequencies of the open form (1KY4), closed form (1K0U), and closed−twisted form (1A7A) obtained from the BNM calculations are presented in Table 2. The frequencies of the open form, in the 1.4−1.7 cm^{-1} range, tend to be lower than the corresponding ones of the closed conformers, 2.6−3.1 cm^{-1} for the closed form and 1.8−2.6 cm^{-1} for the closed−twisted form. Thus, the calculations predict that the open form should be more flexible than the closed conformers, with larger atomic fluctuation amplitudes. This is in agreement with the trend in the crystallographic *B*-factors.

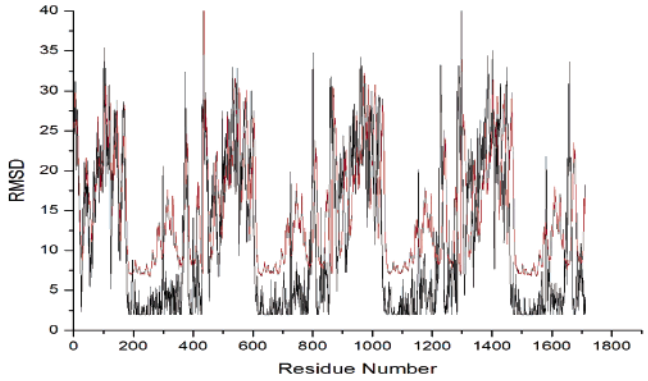

FIGURE 3: Comparison between $\langle R_i^2\rangle^{1/2}$ experimental atomic rms fluctuations (black curve) derived from the corresponding crystallographic isotropic temperature factors, B_i [$\langle \Delta R_i^2\rangle = 3B_i/8\pi^2$ (*23*)], and the calculated rms fluctuations from the first 50 normal modes (red curve) of the C_α atoms in subunit A of the open form of SAHH. Units of angstroms. The correlation coefficient between the two sets of data is 0.89.

BNM Backbone Atom Fluctuations. The overall structural fluctuations of the open form of the protein were investigated by calculating $\langle R_i^2\rangle^{1/2}$ rms position displacements of the C_α atoms due to the first 50 lowest-frequency modes. In Figure 3, the calculated values are compared with the experimental measures of atomic fluctuations obtained from the corresponding crystallographic isotropic temperature factor, B_i [$\langle R_i^2\rangle = 3B_i/8\pi^2$ (*23*)]. The patterns of calculated and observed atomic fluctuations are similar, with a correlation coefficient of 0.89 for 1KY4. The spatial patterns of the calculated and observed atomic fluctuations are shown in Figure 4. Both calculated rms fluctuations and *B*-factors show that the average fluctuations are larger in the substrate-binding domain (SBD, residues 1−180) than in the nucleotide-binding domain (NBD, residues 190−350). This is consistent with the idea that the SBD is the more mobile domain located at the enzyme periphery and moving to open and close the substrate-binding cleft while the NBD is the less mobile domain located at the core of the tetrameric structure. In general, the rms fluctuations are larger in the outside edges of the two domains and are smallest in the inside edges, i.e., the cleft between the two domains, indicating the presence of a cleft opening or closing motion. There are two relatively broad minima in the fluctuation profiles, located at around residues 185 and 353 that connect the two domains. These two regions exhibit rather small amplitude fluctuations in both crystallographic *B*-factors and normal mode motion amplitudes, and may be considered hinge regions for the domain reorientations.

A similar pattern of atomic fluctuations was obtained using the simplified Gaussian normal mode model (*24*) in which the local stiffness of the protein is modeled as being proportional to the number of nearest neighbors. The detailed results are presented in ref *25*.

Open Form Normal Mode Projections: Domain Hinge Bending. By overlaying the backbones of the open (1KY4)

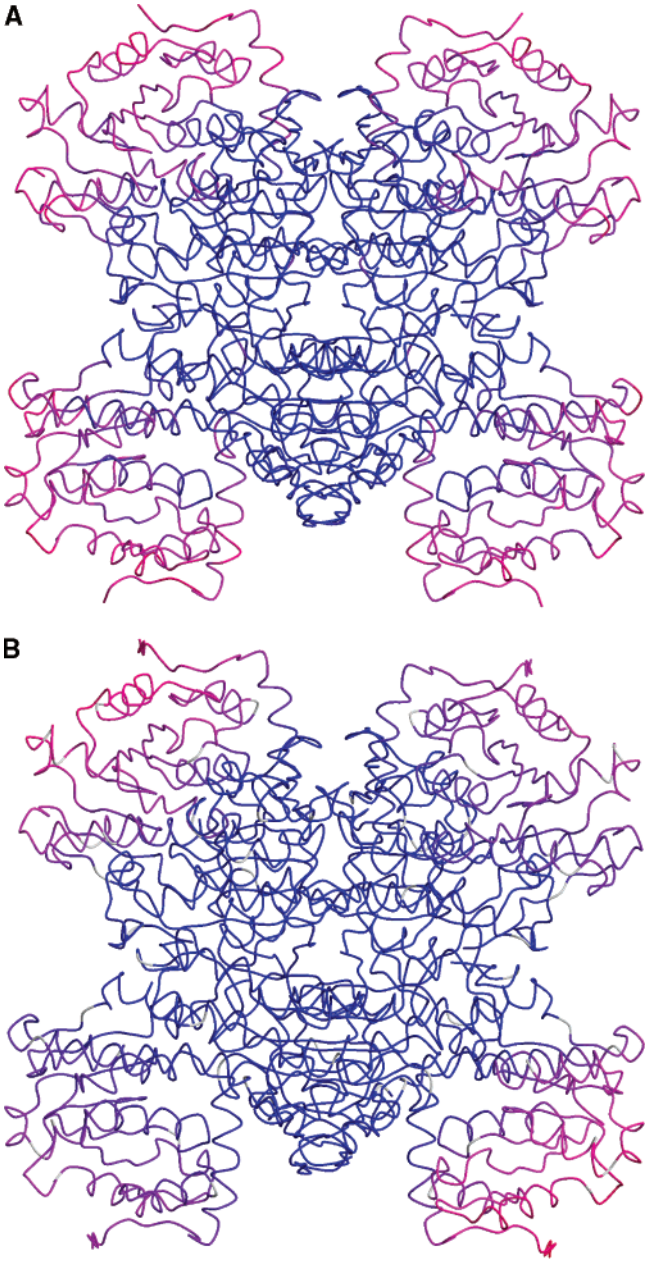

FIGURE 4: Spatial distribution of atomic fluctuations in the open form of SAHH (1KY4). Residues colored according to the *B*-factor (A) or the rms position fluctuation (B) calculated from BNM for the C_α atom: blue for low, green for medium, and red for high. This figure were generated with Molscript (*35*).

and closed (1K0U) forms and taking the differences between Cartesian coordinates of corresponding atoms, we have generated a 3*N*-dimensional vector (*N* is the number of atoms) giving the direction of the open-to-closed conformational transition. The projections of the open form BNM modes on the parts of this vector corresponding to the four individual subunits are presented in Table 3. In the case of ideal tetrahedral symmetry, we can form four symmetrized combinations of the four hinge bending motions u_i (i = A, B, C, or D) with the fully symmetric normalized combination being $(u_A + u_B + u_C + u_D)/2$, and the remaining ones differing from it by changes in sign (*26*). If the domain hinge bending motions were able to fully account for the structural transition, we would expect contributions of 25% from each subunit for modes describing motions corresponding exactly

Table 3: Contributions (%) from Individual Subunits to Normal Mode Projections on the Open-to-Closed Conformational Transition[a]

		subunit A	subunit B	subunit C	subunit D
1KY4	mode 7	14	31	28	11
	mode 8	5	29	28	2
	mode 9	24	5	9	24
	mode 10	21	2	4	30
	modes 1−50	88	88	88	90
1K0U	mode 7	14	12	13	15
	mode 8	1	2	2	1
	mode 9	4	2	6	1
	mode 10	1	7	2	4
	modes 1−50	81	82	82	83
1A7A	mode 7	4	1	4	1
	mode 9	9	15	9	15
	mode 10	0	7	0	7
	mode 11	2	1	2	1
	mode 17	13	0	12	0
	modes 1−50	83	81	83	80

[a] Values calculated from dot products of normalized 3*N*-dimensional vectors of normal modes and structural displacement. 1KY4 modes, open conformer: displacement vector from 1KY4 to 1K0U. 1K0U modes, closed conformer: displacement vector from 1K0U to 1KY4. 1A7A modes, closed−twisted conformer: displacement vector from 1A7A to 1KY4.

to the structural change occurring in the open-to-closed conformational transition. Deviations of the projections from the ideal values of 25% may have two causes: deviations of the SAHH structure from tetrahedral symmetry and differences between the normal mode motions and the direction of the structural transition. Modes 7−10 of the open form have projections that roughly match the expected tetrahedral pattern, with some values above and some below 25%. Thus, the lowest-frequency vibrations of the open form may be considered to be mostly combinations of subunit motions along the direction of the open-to-closed transition.

This finding leads to three important conclusions. First, the three-dimensional shape and intramolecular interactions of the open form are such that its lowest-frequency vibrations, describing the collective motions of largest amplitude, correspond to domain hinge bending. Indeed, the lowest-frequency vibration, mode 7 of the open form, describes a motion almost exactly along the transition vector from open structure 1KY4 to closed structure 1K0U. The second conclusion is that, as the first four modes are mostly combinations of the hinge bends, the subunit hinge motions are uncoupled from the other protein modes in open structure 1KY4. Finally, since the frequencies of modes 7−10 are similar (Table 2), the coupling between the hinge bends in the four subunits is weak.

Our result that the low-frequency vibrations of the open form of the enzyme occur in the direction of the open-to-closed conformational transition is a new example of what appears to be a more general trend. Similar effects have been found for ~20 proteins, with methods including standard normal mode analysis and BNM (*20*), as well as a simplified elastic model (*27*).

Closed Form Normal Mode Projections: Coupled Subunit Motions. Projections of the normal modes of closed form 1K0U on the same closed-to-open structural transition (from 1K0U to 1KY4) give markedly different results. Only the lowest-frequency vibrational mode, mode 7, has a large contribution from subunit hinge bending. Overall, this mode

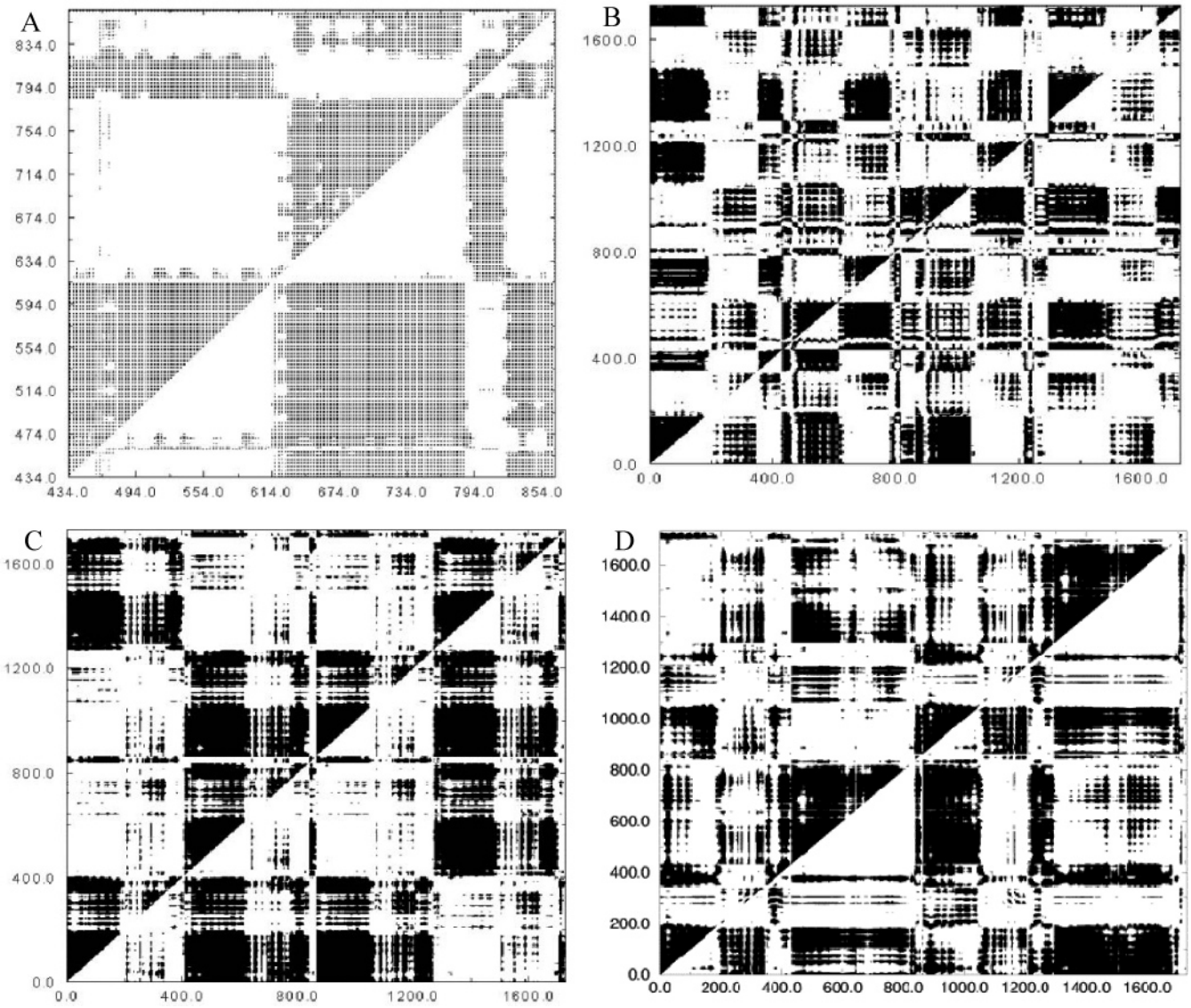

FIGURE 5: Normalized covariance matrices for open form 1KY4, subunit B shown to illustrate the characteristic pattern of domain hinge bending fluctuations (A), at the tetramer level (B), and for closed form 1K0U (C) and 1A7A (D). The *X* and *Y* axes show residue numbers. Positive correlations between residue motions are denoted with a dot above the diagonal and negative correlations below the diagonal.

has a 54% overlap with the direction of the structural transition. Among the remaining low-frequency modes, the contributions from hinge bending deformations are small. The results for the closed−twisted 1A7A structure are similar. Projections of the low-frequency 1A7A normal modes on the closed-to-open structural transition (from 1A7A to 1KY4) tend to be small, with the largest overlap being 50% for mode 9. Overall, the low-frequency vibrations of the closed forms are markedly different from those of the open conformer. In both closed structures, there is a low-frequency vibration with a significant component (50−54%) along the open-to-closed structural transition. Because of the higher frequencies of the closed form modes, the amplitudes of these motions will be smaller than in the open conformer. Further, the hinge bending deformations of the closed forms contribute to many normal modes, indicating strong coupling of the hinge bends to each other and to other low-frequency vibrations. Thus, the shape and intermolecular interactions of the closed forms are such that the lowest-frequency normal modes, corresponding to the collective motion with the largest amplitude, involve some motion along the direction of the open-to-closed structural transition and coupling of deformations in the individual domains and subunits.

Normal Mode Projections: Dimer Reorientation. By overlaying the backbones of the closed (1K0U) and closed−twisted (1A7A) forms and taking the differences between Cartesian coordinates of corresponding atoms, we have generated a 3*N*-dimensional vector giving the direction of the conformational transition between these forms, which mainly involves a 14° dimer twist (Table 1). Among the vibrational normal modes of closed−twisted structure 1A7A, there are none that have a contribution above 16% along the 1A7A-to-1K0U transition. Thus, for this form of SAHH, there is no characteristic collective motion corresponding to dimer twisting.

Correlations between Structural Elements. The covariance matrices describing correlations between residue fluctuations in the lowest-frequency modes of three forms of SAHH are displayed in Figure 5A−D; more results are shown on our Web site (*21*). The diagrams in Figure 5 allow easy identification of correlated motions of different parts of the protein structure. The residue numbers for a chosen sequence

Table 4: Force Constant Matrix and Covariance Matrix in the Subspace of Hinge Bending Motions of the Four Subunits of Open Form 1KY4

Force Constant Matrix, $\mathbf{F}_u$ (kcal mol^{-1} deg^{-2})				
	subunit A	subunit B	subunit C	subunit D
subunit A	**1.67**	0.20	−0.14	0.06
subunit B	0.20	**2.00**	0.28	−0.09
subunit C	−0.14	0.28	**2.02**	0.14
subunit D	0.06	−0.09	0.14	**1.74**
Covariance Matrix $\mathbf{C}_u$ (deg^2)				
	subunit A	subunit B	subunit C	subunit D
subunit A	**0.37**	−0.04	0.03	−0.02
subunit B	−0.04	**0.31**	−0.05	0.02
subunit C	0.03	−0.05	**0.31**	−0.03
subunit D	−0.02	0.02	−0.03	**0.35**

are plotted, increasing upward along the ordinate and rightward along the abscissa. For any two protein fragments, there will be blocks of cells marked with dots, located above the diagonal when residues within the fragments move in a correlated manner and below the diagonal when their motions are anticorrelated (see the legend of Figure 5). The pattern of motion corresponding to domain hinge bending is illustrated in Figure 5A, on the example of mode 8 for open form subunit B. The two main triangular blocks above the diagonal show that the two large domains, SBD (residues 1−180) and CBD (residues 190−350), move essentially as rigid bodies. The large square below the diagonal shows that the SBD and the CBD move with opposite phases, as expected in a hinge bend. Additionally, we see the C-terminal tail (residues 360−432) may be separated into two parts, with one (residues 360−395) correlated with the SBD and the other (residues 396−432) correlated with the CBD. The regions of low mobility corresponding to the hinges may be clearly seen around residues 180 and 353. A pattern of the hinge bending type is found in the four lowest-frequency modes of the open form (Figure 5B), and several low-frequency modes of the closed and closed−twisted forms (*21*). Covariance matrices for mode 7 of closed structure 1K0U (Figure 5C) and mode 7 of closed−twisted structure 1A7A (Figure 5D) show examples of collective motions spanning whole subunits and dimers of the tetrameric protein. These covariance matrices are in general accord with our projection analysis described above, indicating that the lowest-frequency collective motions are primarily combinations of domain hinge bends in the open conformation and coupled hinge bends and subunit and dimer reorientations in the closed forms.

Hinge Bending Force Constants. We have determined that the four lowest-frequency vibrational modes of the SAHH open form are primarily combinations of domain hinge bending deformations of the four subunits of the protein. Assuming that these modes correspond to pure combinations of hinge bends which are uncoupled from all other protein motions, we have calculated the force constant matrix in the hinge bending coordinates, as described in Methods. The force constant matrix is presented in Table 4. The average diagonal force constant, describing the stiffness of an individual subunit hinge, is 1.86 kcal mol^{-1} deg^{-2}. This value is comparable to the force constant determined for lysozyme hinge bending (*11*). The off-diagonal force constants, describing interactions between hinge bends on different subunits, tend to be about 1 order of magnitude smaller than the diagonal elements. Thus, the interactions between subunit hinge bending deformations tend to be small, as expected from the similarity of the first four normal mode frequencies. The largest interaction force constants are within the two dimers of SAHH. The average interaction force constant between subunits in the A−B and C−D dimers is 0.17 kcal mol^{-1} deg^{-2}. The positive value of this force constant means that it is somewhat more costly to deform both hinges in a dimer simultaneously than to introduce two separate deformations. From the force constant matrix, we can also obtain the covariance matrix describing average amplitudes of the hinge bending motions (Table 4). The average diagonal element is ∼0.34 deg^2, corresponding to a mean amplitude of ∼0.6° at 300 K. The covariance matrix also shows a weak anticorrelation of the deformations within the A−B and C−D subunits, in agreement with the discussion above.

Relation between Local Structural Fluctuations and Global Structural Transition. Normal modes represent collective motions around a local minimum on the molecular potential energy surface, while structural transitions represent large-scale motions between different local minima (*28*). In general, any kind of internal structural change may be expressed as a combination of all possible normal modes, which form an alternative coordinate system to the usual Cartesian coordinates. What is interesting in our results is that the lowest-frequency vibrational modes of SAHH exhibit significant overlap with the vectors defining the structural transitions. Thus, the mechanical properties of the protein are such that the collective motions with the largest amplitudes occur in the direction of the structural transition. In our in vacuo normal mode calculations, the amplitudes of the structural fluctuations for the open form hinge bending motions are close to 1°, and the time scales are ∼20 ps (for frequencies of 1.5 cm^{-1}). The BNM fluctuation amplitude is much smaller than the 18° rotation needed to bring the substrate-binding domain from the open to the closed conformation. Also, fluorescence studies reveal a time scale of ∼25 ns for domain reorientations of substrate-free SAHH in solution (*8*), 3 orders of magnitude slower than the slowest vibration.

One reason the vibrational time scales and amplitudes may be underestimated is that the calculations have been performed in a vacuum. It is well-known that in the presence of solvent the effective intramolecular potential becomes "softer", leading to motions with lower frequencies and larger amplitude (*11*). To obtain a vibrational frequency that is 10^3 times lower, solvation would have to decrease the effective hinge bending force constant by a factor of 10^6, which is unlikely. Friction is another solvent effect neglected in our vacuum simulations. Studies of inclusion of frictional effects indicate that low-frequency vibrations should be overdamped in the presence of a solvent (*29*, *30*). These modes would thus describe nonperiodic motion, with effective time scales longer than that dictated by the harmonic frequencies. However, friction does not influence the amplitude of the motions.

These considerations suggest that to explain the time scale and amplitude of the SAHH large-scale structural transitions, we should treat it not as an elastic deformation but as a more complex process involving either diffusion over the potential energy surface or crossing of a barrier between the minima

corresponding to the identified stable states (*28*, *31*). We can thus expect the harmonic vibrations to describe only the initial stages of the conformational transitions. The presence of these local vibrations promotes larger global structural changes in the enzyme, and different global conformers may be stabilized by specific interactions at various stages of the enzymatic cycle.

Overall, several interesting conclusions about the enzymatic mechanism of SAHH may be drawn from our normal mode analysis. The presence of low-frequency hinge bending vibrations in the open form suggests that the 25 ns time scale motion observed by fluorescence in substrate-free SAHH represents hinge bending type motions, involving fluctuations along the pathway between the open and closed conformations. In the presence of substrate, the hinge bending motions will not be completely abolished, but rather should occur on the time scale of enzyme turnover, as SAHH binds the substrate and releases the product. The turnover is in the second range (*32*), so probe reorientations on this time scale would not be seen in the fluorescence depolarization experiments because of the probe fluorescence lifetime (*8*).

The second interesting finding from the normal mode analysis is that the hinge bending vibrations are mostly independent of each other and of other protein structural fluctuations in the open form, while vibrations representing domain and subunit reorientations are strongly coupled in the closed forms. This suggests that substrate binding to the open subunits might proceed independently, while any structural changes in the closed form should exhibit correlations between subunits; i.e., the mechanical properties of the closed conformations should induce cooperativity between the SAHH subunits. This is in agreement with kinetic measurements, which indicate that the enzyme exhibits cooperativity, and may be considered a dimer of dimers.

There is suggestive but not definitive evidence of subunit cooperativity for human SAHH. For example, a mechanism-based inhibitor reacts with half of the active sites in the enzyme but produces full inactivation (*33*). The steady state kinetics of hydrolysis and synthesis of AdoHcy show, in our hands, at best weak indications of cooperativity (e.g., Hill coefficients of 1.2), but some active site and cofactor binding site mutants produce more definite indications, with Hill coefficients of 1.4−2.

CONCLUSIONS

We present an analysis of the structure and fluctuations of SAHH, aimed at improving our understanding of the biological function of this interesting protein. Previous analysis of the crystal structures indicated the presence of two forms of SAHH, the open form, characteristic of the substrate-free enzyme, and the closed form, found in enzyme−inhibitor complexes (*5*, *15*, *22*). By comparing the available three-dimensional tetramer structures, we were able to distinguish several interesting features. In all four known SAHH−inhibitor complex structures, the clefts between the large domains in the four subunits are closed, isolating the inhibitor bound in the active site from the bulk solvent. Interestingly, the two SAHH−inhibitor complexes that correspond to the central intermediate of the enzymatic cycle, 4′,5′-didehydro-5′-deoxy-3′-ketoadenosine, tend to exhibit the most tightly closed subunit hinges. This may be related to the previously identified increased cofactor−inhibitor distance in these structures, which increases the barrier for product release and suppresses an abortive oxidative side reaction. Additionally, we have found that three enzyme inhibitor complexes, 1K0U, 1LI4, and 1KY5, take on a closed conformation that differs from the open conformer mainly by closure of the interdomain clefts of the four subunits. However, the fourth complex, 1A7A, exists in a closed−twisted conformation, which is obtained from the closed structure by a 14° relative reorientation of the two subunit dimers. The closed−twisted conformer has been found only in one complex, the 1A7A structure involving the inhibitor DHCeA, chemically corresponding to the central intermediate of the enzymatic cycle. Since the 1LI4 complex, which also corresponds to the central intermediate, does not exhibit a significant dimer twist, the role of the closed−twisted structure in the catalytic mechanism of SAHH in not clear, based on the available data.

Further, we performed block normal mode analysis of the tetramers of SAHH in the three conformations, to explore the structural fluctuations of these states. For the open form, we find that the four lowest-frequency normal modes, corresponding to the collective motions of the protein with the largest amplitudes, are essentially combinations of the hinge bending deformations of the individual subunits. Thus, the mechanical properties of the open structure of SAHH lead to the presence of structural fluctuations in the direction of the open-to-closed vibrational transition. In our calculations, the typical hinge bending force constant was ∼2 kcal mol^{-1} deg^{-2}, the amplitude of motion ∼1° at room temperature, and the time scale ∼20 ps. The vibrational amplitude is much smaller than the 18° reorientation found in the open-to-closed structural transition and the time scale much shorter than the 25 ns domain reorientation observed in fluorescence depolarization studies. This suggests that the open-to-closed structural transition in SAHH cannot be described as an elastic deformation, but should be treated as a more complex motion, involving diffusive or activated dynamics between two stable states. The collective fluctuations described by the normal modes represent local motions along the reaction coordinates that could promote the transition. The transitions between the stable protein conformers appear to be driven by interactions with the substrate, intermediates, and product in the enzymatic reaction (*7*). Our finding of a correlation between structural fluctuations of the open form of SAHH and the open-to-closed structural transition is a further example of a more widespread phenomenon, confirmed for ∼20 different proteins (*27*).

Our normal mode analysis clearly shows that hinge bending fluctuations are an important feature of the open structure of SAHH. This supports the interpretation of the 25 ns time scale reorientation found in fluorescence depolarization studies as a hinge bending motion. Both structural and normal mode analyses identify residues in the 180−190 and 350−360 regions as the hinges of SAHH, i.e., the regions that connect the large rigid domains of the protein. This leads us to believe that these regions should be important for the biological role of SAHH. Indeed, several residues in the first region [Asn 181, Lys 186, Asp 190, and Asn 191 (*34*)] are part of the active site. The role of the residues in the second region, 350−360, has not been studied previously. We are currently analyzing the influence of point

mutations in this region on the enzymatic activity of SAHH through site-directed mutagenesis and kinetics studies.

The normal mode analysis reveals markedly different mechanical properties of the open and closed structures of SAHH. In the open form, the hinge bending motions tend to be independent of one another and of other protein vibrations. In contrast, in the closed form, the hinge bending deformations tend to be coupled to one another and other low-frequency vibrations, including subunit reorientations. These properties might be used to explain the cooperativity observed in the enzyme kinetics. The presence of substrate stabilizes SAHH in the closed conformations. Any structural changes that occur in one of the four active sites in the course of the enzymatic reaction should be transmitted to the other sites through the mechanical coupling that is characteristic of the closed forms.

Our normal mode calculations are only able to describe local harmonic vibrations of the protein structures. To characterize the larger motions involved in the anharmonic structural transitions, we are pursuing investigations of the open-to-closed transition of SAHH using the stochastic differential equation method of R. Elber (*31*).

ACKNOWLEDGMENT

We are grateful to Prof. Qiang Cui (University of Wisconsin, Madison, WI) for providing an early release of the BNM computer code and help with setting up the calculations and to Dr. Lynne Howell (Hospital for Sick Children, Toronto, ON) for providing the coordinates of the tetramer of the 1LI4 structure.

REFERENCES

1. Schnyder, G., Roffi, M., Pin, R., Flammer, Y., Lange, H., Eberli, F. R., Meier, B., Turi, Z. G., and Hess, O. M. (2001) Decreased rate of coronary restenosis after lowering of plasma homocysteine levels, *N. Engl. J. Med. 345*, 1593−1600.
2. Ueland, P. M., Resfsum, H., and Brattstrom, L. (1992) in *Plasma Homocysteine and Cardiovascular Disease* (Francis, R. B., Jr., Ed.) pp 183−196, Marcel Dekker, New York.
3. Robins, M. J., Wnuk, S. F., Yang, X., Yuan, C. S., Borchardt, R. T., Balzarini, J., and De Clercq, E. (1998) Inactivation of *S*-adenosyl-L-homocysteine hydrolase and antiviral activity with 5′,5′,6′,6′-tetradehydro-6′-deoxy-6′-halohomoadenosine analogues (4′-haloacetylene analogues derived from adenosine), *J. Med. Chem. 41*, 3857−3864.
4. Yang, X., and Borchardt, R. T. (2000) Overexpression, purification, and characterization of S-adenosylhomocysteine hydrolase from *Leishmania donovani*, *Arch. Biochem. Biophys. 15*, 272−280.
5. Turner, M. A., Yuan, C. S., Borchardt, R. T., Hershfield, M. S., Smith, G. D., and Howell, P. L. (1998) Structure determination of selenomethionyl *S*-adenosylhomocysteine hydrolase using data at a single wavelength, *Nat. Struct. Biol. 5*, 369−376.
6. Hu, Y., Komoto, J., Huang, Y., Gomi, T., Ogawa, H., Takata, Y., Fujioka, M., and Takusagawa, F. (1999) Crystal structure of *S*-adenosylhomocysteine hydrolase from rat liver, *Biochemistry 38*, 8323−8333.
7. Yang, X., Hu, Y., Yin, D. H., Turner, M. A., Wang, M., Borchardt, R. T., Howell, P. L., Kuczera, K., and Schowen, R. L. (2003) Catalytic strategy of *S*-adenosyl-L-homocysteine hydrolase: Transition-state stabilization and the avoidance of abortive reactions, *Biochemistry 42*, 1900−1909.
8. Yin, D., Yang, X., Hu, Y., Kuczera, K., Schowen, R. L., Borchardt, R. T., and Squier, T. C. (2000) Substrate binding stabilizes *S*-adenosylhomocysteine hydrolase in a closed conformation, *Biochemistry 39*, 9811−9818.
9. Huber, R., and Bennett, W. S., Jr. (1983) Functional significance of flexibility in proteins, *Biopolymers 22*, 261−279.
10. Ma, J., and Karplus, M. (1998) The allosteric mechanism of the chaperonin GroEL: A dynamic analysis, *Proc. Natl. Acad. Sci. U.S.A. 95*, 8502−8507.
11. Brooks, C. L., III, Karplus, M., and Pettitt, B. M. (1988) *Proteins: A theoretical perspective of dynamics, structure and thermodynamics*, Wiley and Sons, New York.
12. Case, D. A. (1998) The use of chemical shifts and their anisotropies in biomolecular structure determination, *Curr. Opin. Struct. Biol. 8*, 624−630.
13. Tama, F., Gadea, F. X., Marques, O., and Sanejouand, Y. H. (2000) Building-block approach for determining low-frequency normal modes of macromolecules, *Proteins 41*, 1−7.
14. Li, G., and Cui, Q. (2002) A coarse-grained normal mode approach for macromolecules: An efficient implementation and application to Ca^{2+}-ATPase, *Biophys. J. 83*, 2457−2474.
15. Huang, Y., Komoto, J., Takata, Y., Powell, D. R., Gomi, T., Ogawa, H., Fujioka, M., and Takusagawa, F. (2002) Inhibition of *S*-adenosylhomocysteine hydrolase by acyclic sugar adenosine analogue D-eritadenine. Crystal structure of *S*-adenosylhomocysteine hydrolase complexed with D-eritadenine, *J. Biol. Chem. 277*, 7477−7482.
16. Brooks, B. R., Olafson, B. D., States, D. J., Swaminathan, S., and Karplus, M. (1983) CHARMM: A program for macromolecular energy, minimization and dynamics calculations, *J. Comput. Chem. 4*, 187−217.
17. Brunger, A. T., and Karplus, M. (1988) Polar hydrogen positions in proteins: Empirical energy placement and neutron diffraction comparison, *Proteins 4*, 148−156.
18. MacKerell, A. D., Jr., Bashford, D., Bellott, M., Dunbrack, R. L., Jr., Evanseck, J. D., Field, M. J., Fischer, S., Gao, J., Guo, H., Ha, S., Joseph-McCarthy, D., Kuchnir, L., Kuczera, K., Lau, F. T. K., Mattos, C., Michnick, S., Ngo, T., Nguyen, D. T., Prodhom, B., Reiher, W. E., III, Roux, B., Schlenkrich, M., Smith, J. C., Stote, R., Straub, J., Watanabe, M., Wiorkiewicz-Kuczera, J., Yin, D., and Karplus, M. (1998) All-atom empirical potential for molecular modeling and dynamics studies of proteins, *J. Phys. Chem. B 102*, 3586−3616.
19. Pavelites, J. J., Bash, P. A., Gao, J., and MacKerell, A. D., Jr. (1997) A Molecular Mechanics Force Field for NAD^+, NADH, and the Pyrophosphate Groups of Nucleotides, *J. Comput. Chem. 18*, 221−239.
20. Durand, P. T. G., and Sanejouand, Y.-H. (1994) A new approach for determining low-frequency normal modes in macromolecules, *Biopolymers 34*, 759−771.
21. Wang, M., and Kuczera, K. (2004) Images and animations from SAHH normal mode analysis, http:/assam.chem.ku.edu/∼kuczera/sahbnm/bnm.html.
22. Takata, Y., Yamada, T., Huang, Y., Komoto, J., Gomi, T., Ogawa, H., Fujioka, M., and Takusagawa, F. (2002) Catalytic mechanism of *S*-adenosylhomocysteine hydrolase. Site-directed mutagenesis of Asp-130, Lys-185, Asp-189, and Asn-190, *J. Biol. Chem. 277*, 22670−22676.
23. Weaver, L. H., and Matthews, B. W. (1987) Structure of bacteriophage T4 lysozyme refined at 1.7 Å resolution, *J. Mol. Biol. 193*, 189−199.
24. Haliloglu, T., Bahar, I., and Erman, B. (1997) Gaussian Dynamics of Folded Proteins, *Phys. Rev. Lett. 79*, 3090−3093.
25. Wang, M. (2005) Studies of role of hinge regions in structure, dynamics and mechanism of *S*-adenosylhomocysteine hydrolase, Ph.D. Thesis, University of Kansas, Lawrence, KS.
26. Bright Wilson, E., Jr., Decius, J. C., and Cross, P. C. (1980) *Molecular Vibrations: The Theory of Infrared and Raman Vibrational Spectra*, Dover Publications, New York.
27. Tama, F., and Sanejouand, Y.-H. (2001) Conformational change of proteins arising from normal mode calculations, *Protein Eng. 14*, 1−6.
28. Elber, R. (1996) Reaction path studies in biological molecules, in *Recent Developments in Theoretical Studies of Proteins* (Elber, R., Ed.) pp 65−135, World Scientific, Singapore.
29. Lamm, G., and Szabo, A. (1986) Langevin modes of macromolecules, *J. Chem. Phys. 85*, 7334−7348.
30. Hayward, S., Kitao, A., Hirata, F., and Go, N. (1993) Effect of solvent on collective motions in globular proteins, *J. Mol. Biol. 234*, 1207−1217.
31. Siva, K., and Elber, R. (2003) Ion permeation through the gramicidin channel: Atomically detailed modeling by the stochastic difference equation, *Proteins 50*, 63−80.

32. Porter, D. J., and Boyd, F. L. (1991) Mechanism of bovine liver *S*-adenosylhomocysteine hydrolase. Steady-state and pre-steadystate kinetic analysis, *J. Biol. Chem. 266*, 21616−21625.
33. Yuan, C.-S., Wnuk, S. F., Robins, M. J., and Borchardt, R. T. (1998) A novel mechanism-based inhibitor (6′-bromo-5′,6′-didehydro-6′-deoxy-6′-fluorohomoadenosine) that covalently modifies human placental *S*-adenosylhomocysteine hydrolase, *J. Biol. Chem*. *273*, 18191−18198.
34. Elrod, P., Zhang, J., Yang, X., Yin, D., Hu, Y., Borchardt, R. T., and Schowen, R. L. (2002) Contributions of active site residues to the partial and overall catalytic activities of human *S*-adenosylhomocysteine hydrolase, *Biochemistry 41*, 8134−8142.
35. Kraulis, P. (1991) MOLSCRIPT: A program to produce both detailed and schematic plots of protein structures, *J. Appl. Crystallogr*. *24*, 946−950.

BI047524M